

# SPH Formulation and Fluid-Solid Interface Model for the Fully Compressible Interaction of Dissimilar Materials

Jason M. Pearl, Cody D. Raskin, J. Michael Owen

Design Physics Department  
Lawrence Livermore National Laboratory  
Livermore, CA, USA  
pearl3@llnl.gov

**Abstract**—An energy-conserving density-energy SPH formulation suitable for modeling the interaction of materials with large differences in compressibility and density is overviewed. The formulation includes a material interface model that admits discontinuities in the velocity gradient, as well as slip and no-slip interface conditions. Results using the new formulation are presented for several standard density discontinuity test-case problems.

## I. INTRODUCTION

The challenges associated with modeling density discontinuities with SPH are well documented [1]. At contact discontinuities, traditional SPH formulations produce artificial surface tension that suppresses the growth of hydrodynamic instabilities.

Several methods have been developed to remedy these deficiencies. Alternate formulations were derived that replace the density as the fundamental kernel-smoothed field [2], [3]. Pressure-based formulations (PSPH) can provide smooth pressure fields at contact discontinuities but require the use of iterative solvers to interface with arbitrary equations of state [4]. Certain density-energy formulations can also yield good behavior at density discontinuities [5]–[7]. Another approach is to add thermal diffusion to a traditional SPH formulation [8].

A problem that is encountered less frequently is a step change in compressibility. Similar to density discontinuities, compressibility discontinuities require special care for an SPH formulation FSISPH to give physical results. Here we describe a new density-energy SPH formulation (FSISPH) suitable for highly dynamic interactions of dissimilar materials with drastically different compressibilities. The method was originally developed to model the break up of asteroids in the atmosphere and thus was designed to accommodate arbitrary equations of state (EOS), hypersonic mach numbers, density discontinuities greater than 3 order of magnitude, and slip interface conditions. FSISPH is part of Spherical++ and is publicly available: <https://github.com/LLNL/spherical>.

## II. GOVERNING EQUATIONS

In the Lagrangian frame the evolution of an elastic perfectly-plastic material can be described according to Eqns. 1 - 7 [9].

The Cauchy stress tensor,  $\sigma$ , is partitioned into a deviatoric  $S$  and hydrostatic component  $P\mathbf{I}$  – scalar pressure multiplied by the identity matrix.

$$\sigma = S - PI \quad (1)$$

The velocity gradient tensor is divided into its symmetric component, the deformation  $\dot{\epsilon}$ , and antisymmetric component, the rotation  $\mathbf{R}$ . The variable  $\mathbf{v}$  is the velocity.

$$\dot{\epsilon} = \frac{1}{2}(\nabla \mathbf{v} + \nabla \mathbf{v}^T) \quad (2)$$

$$\mathbf{R} = \frac{1}{2}(\nabla \mathbf{v} - \nabla \mathbf{v}^T) \quad (3)$$

The continuity, momentum conservation, and energy conservation equations are shown in Eqns. 4 - 6 with  $\rho$  being the mass density and  $u$  the specific thermal energy.

$$\frac{D\rho}{Dt} = -\rho \nabla \cdot \mathbf{v} \quad (4)$$

$$\rho \frac{D\mathbf{v}}{Dt} = \nabla \cdot \sigma \quad (5)$$

$$\rho \frac{Du}{Dt} = \sigma : \dot{\epsilon} \quad (6)$$

The time evolution of the deviatoric stress tensor is governed by Hooke's Law with additional terms to account for material rotation. The shear modulus is represented by  $\mu$ .

$$\frac{DS}{Dt} = 2\mu(\dot{\epsilon} - Tr(\dot{\epsilon})\mathbf{I}) + \mathbf{S}\mathbf{R}^T + \mathbf{R}\mathbf{S}^T \quad (7)$$

The set of equation is closed by an equation of state characterizing the pressure  $P = P(\rho, u)$  and supplemented by a strength model characterizing the yield strength, and shear modulus in terms of the state.

## III. SPH DISCRETIZATION

### A. Acceleration

For a given pair interaction, the acceleration can be broken down into the specific acceleration contributed by each particle, Eqn. 8, in which  $\Pi_{ij}$  is the artificial viscosity. The

kernel gradient is written in functional form here to define our convention.

$$\mathbf{a}_i = \left( \frac{\boldsymbol{\sigma}_i}{\rho_i \rho_j} - \frac{\mathbf{\Pi}_{ij}}{2} \right) \cdot \nabla W_i(|\mathbf{r}_i - \mathbf{r}_j|, h_i) \quad (8)$$

$$\frac{D\mathbf{v}_i}{Dt} = \sum_j m_j (\mathbf{a}_i - \mathbf{a}_j) \quad (9)$$

*1) Energy Conservation and Continuity:* The compatible energy formulation of Owen [10] is used to enforce energy conservation to machine precision. This formulation requires the half-step velocity. In this implementation, the half-step velocity is calculated according to Eqn. 10 by assessing Eqn. 9 in a primary loop over the node-pairs. This allows the half-step velocity to be used in continuity equation as well – Eqn 11. This provides better consistency between the continuity and energy conservation equations.

$$\mathbf{v}_i^{1/2} = \mathbf{v}_i + \frac{D\mathbf{v}_i}{Dt} \frac{\Delta t}{2} \quad (10)$$

At material interfaces large step jumps in compressibility can occur. To more accurately resolve this type of discontinuity we introduce an intermediate interface velocity to Eqn. 11. This allows for a discontinuous treatment of the velocity gradient between interacting pairs.

$$\frac{D\rho_i}{Dt} = -2\rho_i \sum_j \frac{m_j}{\rho_j} (\mathbf{v}_i^{1/2} - \mathbf{v}_*^{1/2}) \cdot \nabla W_i \quad (11)$$

Energy conservation is rigorously enforced by partitioning the total pairwise work in a manner *most* consistent with our continuity implementation. In Eqn. the consistent work on node  $i$  due to the pair interaction is multiplied by  $f_{ij}$ . The fact  $f_{ij}$  adjusts pairwise specific thermal energy derivative to be rigorously conservative. When  $f_{ij}$  is 1 the equations are both consistent and conservative. This occurs when either the velocity interface is taken to be the mean velocity or  $\mathbf{a}_i$  and  $\mathbf{a}_j$  are identical.

$$\frac{Du_i}{Dt} = 2 \sum_j f_{ij} m_j \mathbf{a}_i \cdot (\mathbf{v}_i^{1/2} - \mathbf{v}_*^{1/2}) \quad (12)$$

$$f_{ij} = \frac{(\mathbf{a}_i + \mathbf{a}_j) \cdot (\mathbf{v}_i^{1/2} - \mathbf{v}_j^{1/2})}{2\mathbf{a}_i \cdot (\mathbf{v}_i^{1/2} - \mathbf{v}_*^{1/2}) - 2\mathbf{a}_j \cdot (\mathbf{v}_*^{1/2} - \mathbf{v}_j^{1/2})} \quad (13)$$

### B. Interface State

When interacting pair nodes belong to the same material the mean pair velocity is used as the interface velocity. When the pair nodes belong to different materials, the velocities are broken down into their respective components and treatment varies depending upon the type of interface condition. Equations 14 and 15 define the parallel and perpendicular components respectively.

$$v_i^{\parallel} = \mathbf{v}_i \cdot \hat{\mathbf{r}}_{ij} \quad (14)$$

$$\mathbf{v}_i^{\perp} = \mathbf{v}_i - v_i^{\parallel} \hat{\mathbf{r}}_{ij} \quad (15)$$

The material properties are then used to construct the interface state. For the parallel component in Eqn. 16 the average is weighted by the nodal bulk moduli  $K$ , volumes  $V$ , kernel gradient magnitudes  $\nabla W$ . A derivation of this scheme is show in the appendix. The same scheme but with the shear modulus  $G$  is used for the perpendicular component in Eqn. 17.

$$v_*^{\parallel} = \frac{K_i V_j \nabla W_i v_i^{\parallel} + K_j V_i \nabla W_j v_j^{\parallel}}{K_i V_j \nabla W_i + K_j V_i \nabla W_j} \quad (16)$$

$$\mathbf{v}_*^{\perp} = \frac{G_i V_j \nabla W_i \mathbf{v}_i^{\perp} + G_j V_i \nabla W_j \mathbf{v}_j^{\perp}}{G_i V_j \nabla W_i + G_j V_i \nabla W_j} \quad (17)$$

*1) Slip Condition:* To enforce a slip condition the interface velocity is reconstructed according to Eqn. 20. There are two different interface velocities for the two pair nodes hence the additional subscript.

$$\mathbf{v}_{i*} = v_*^{\parallel} \hat{\mathbf{r}}_i + \mathbf{v}_i^{\perp} \quad (18)$$

The stress state of Eqn 8 is replaced by the density average effective pressure along the line of interaction – Eqn 19. Here  $\hat{\mathbf{n}}$  is the outward facing unit normal of the interface.

$$\boldsymbol{\sigma}_* = \mathbf{I} \frac{\hat{\mathbf{n}}_i \cdot \boldsymbol{\sigma}_i \cdot \hat{\mathbf{n}}_i \rho_j + \hat{\mathbf{n}}_j \cdot \boldsymbol{\sigma}_j \cdot \hat{\mathbf{n}}_j \rho_i}{\rho_i + \rho_j} \quad (19)$$

*2) No-Slip Condition:* To enforce a slip condition the interface velocity is reconstructed according to Eqn. 20.

$$\mathbf{v}_{i*} = v_*^{\parallel} \hat{\mathbf{r}}_{ij} + \mathbf{v}_*^{\perp} \quad (20)$$

The stress state in Eqn 8 is replaced by the density average effective pressure along the line of interaction – Eqn 21

$$\boldsymbol{\sigma}_* = \frac{\boldsymbol{\sigma}_i \rho_j + \boldsymbol{\sigma}_j \rho_i}{\rho_i + \rho_j} \quad (21)$$

Returning to Eqn. 13 with this construction scheme in mind, it can be shown that consistency is only broken when the smoothing scale is different for an interacting node pair spanning a material interface. For nodes in different materials,  $\mathbf{a}_i$  and  $\mathbf{a}_j$  only differ due to variations in the smoothing scale. For nodes within the same material the mean velocity is used as the interface velocity and  $f_{ij} \rightarrow 1$ .

### C. Conservative Diffusion

For stiff equations of state, it is necessary to use the continuity equation to update the particle density instead of the usual summation. For long time intervals however, the continuity-base density field can be prone to checkerboarding and ringing near interfaces. To mitigate these effects a small amount of diffusion is added to state variables  $\rho$  and  $u$  according to Eqns. 22 and 23 respectively. To ensure energy conservation average values are used for the density  $\rho_{ij}$ , sound speed  $c_{ij}$ , smoothing length  $h_{ij}$ , and kernel gradient  $\nabla W_{ij}$ . Coefficients of diffusion,  $C_d$ , of 0.02 are typically suitable for this purpose and all FSISPH results presented here use these values unless otherwise stated.

$$\frac{D\rho_i}{Dt} = -C_d \sum_{j \in c_i = c_j} \frac{m_j (\rho_j - \rho_i) c_{ij} h_{ij} \mathbf{r}_{ij} \cdot \nabla W_{ij}}{\rho_j (r_{ij}^2 + \epsilon)} \quad (22)$$

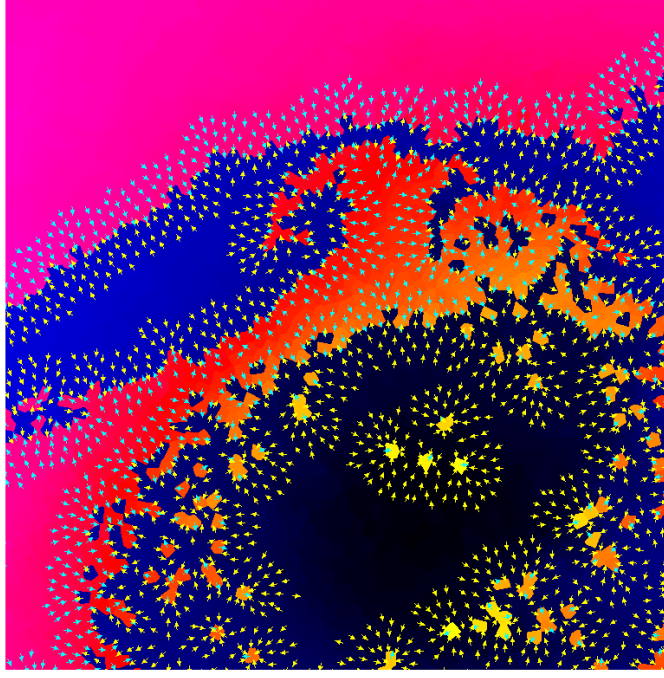


Fig. 1. Interface normals within a Kelvin-Helmholtz roll-up.

$$\frac{Du_i}{Dt} = -C_d \sum_{j \in c_i=c_j} \frac{m_j(u_j - u_i)c_{ij}h_{ij}\mathbf{r}_{ij} \cdot \nabla W_{ij}}{\rho_{ij}(r_{ij}^2 + \epsilon)} \quad (23)$$

#### D. Interface Normals

Interface normals are calculated for nodes that neighbor a different material. A direction vector is calculated according to Eqn. 24. Here we denote different materials by their material index, i.e. color function,  $c$  [11]. The direction vector is then normalized to provide the interface normal for a given node. Interface normals are plotted in Fig. 1.

$$\mathbf{n} = - \sum_{j \in c_i \neq c_j} \frac{m_j}{\rho_j} \nabla W_i \quad (24)$$

#### E. Artificial Viscosity

The Monghan Gingold artificial viscosity Eqn. 27 [12] with Balsara correction  $f_{ij}$  [13] is used.

$$\mu_{ij} = \max \left( \frac{\mathbf{v}_{ij} \cdot \mathbf{r}_{ij} h_{ij}}{r_{ij}^2}, 0 \right) \quad (25)$$

$$\Pi_{ij} = -\frac{f_{ij}}{\rho_{ij}} (\alpha c_{ij} \mu_{ij} + \beta \mu_{ij}^2) \quad (26)$$

When a slip condition is imposed at an interface, the artificial viscosity is reduced using the interface normals according to Eqn 27.

$$\Pi_{ij} \rightarrow \Pi_{ij} (\hat{\mathbf{n}}_i \cdot \hat{\mathbf{v}}_{ij}) (\hat{\mathbf{n}}_j \cdot \hat{\mathbf{v}}_{ij}) \quad (27)$$

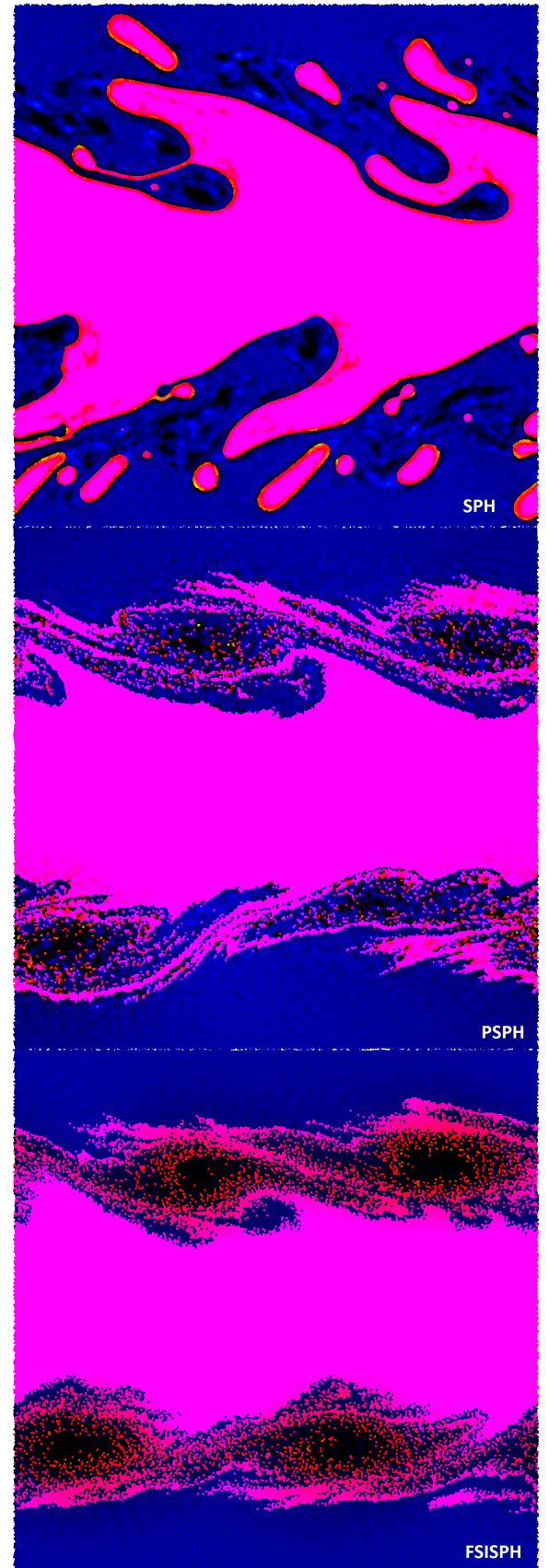
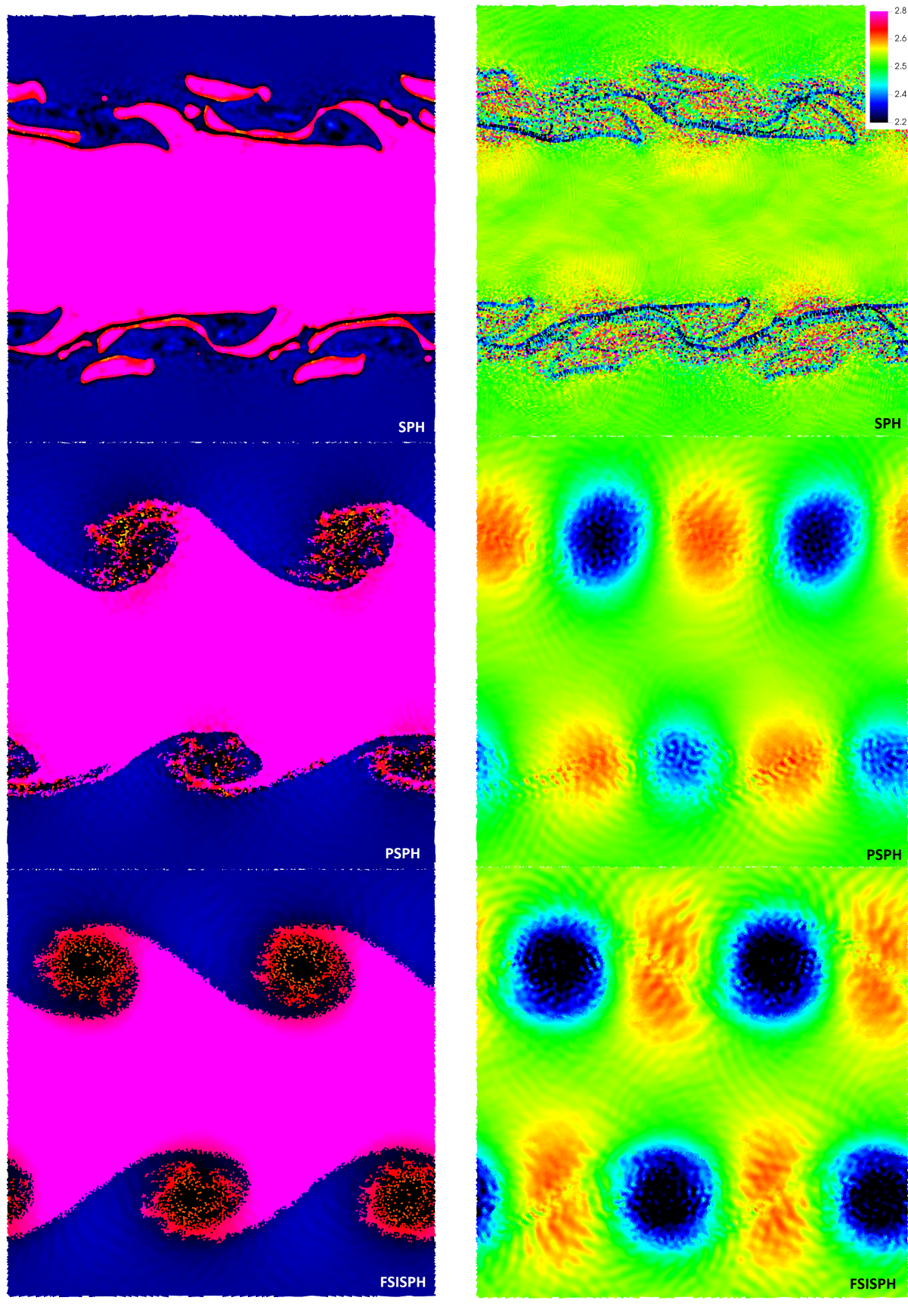


Fig. 2. Density contours for the Kelvin-Helmholtz instability test after  $t = 4\tau_{KH}$ . From top to bottom: SPH, PSPH, FSISPH.



(a) Mass density.

(b) Pressure.

Fig. 3. Kelvin-Helmholtz instability test after  $t = 2\tau_{KH}$ . From top to bottom: SPH, PSPH, FSISPH.

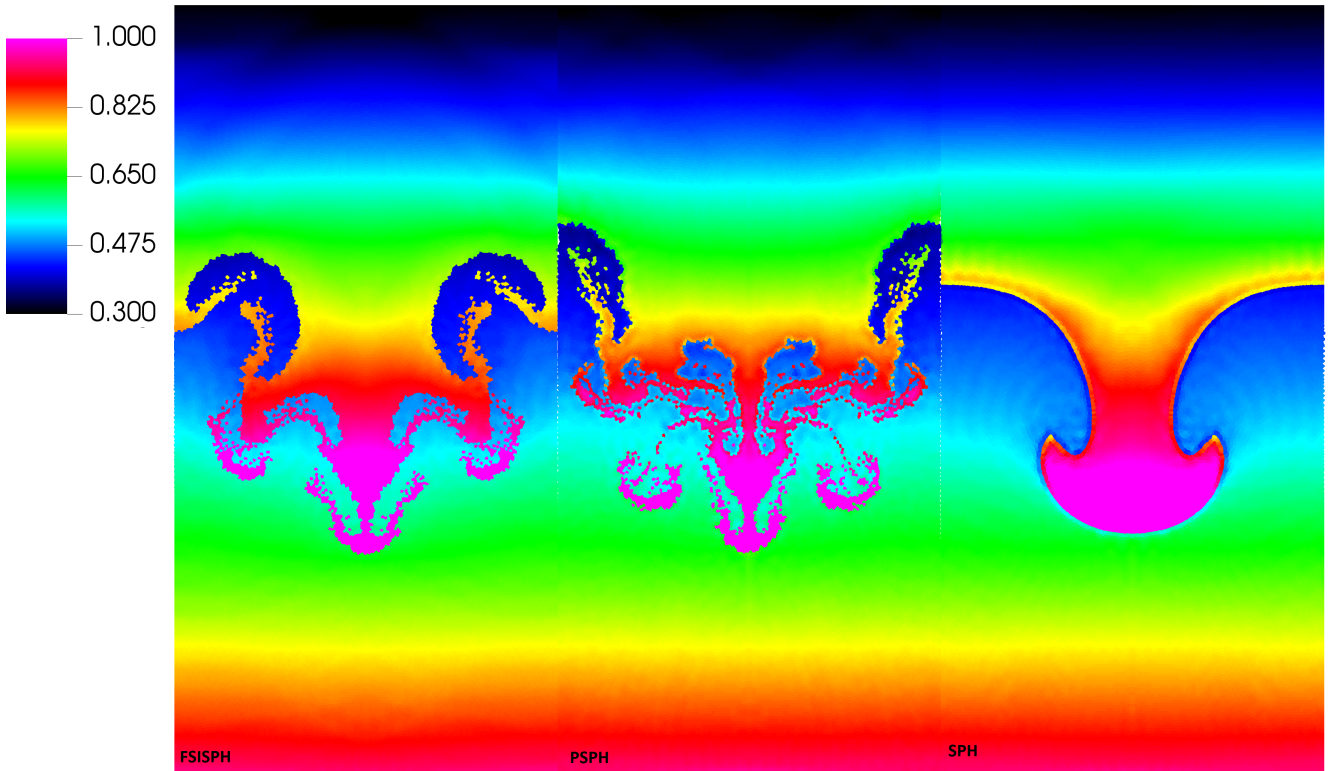


Fig. 4. Density contours for the Rayleigh-Taylor instability after  $t = 5.0$  seconds. From left to right: FSISPH, PSPH, SPH.

#### IV. RESULTS

The proposed FSISPH formulation is compared to traditional SPH [14], and a pressure based formulation PSPH [2] for several common hydrodynamic test-cases. For all simulations, we use the fourth order Wendland kernel [15] and hold artificial viscosity coefficients constant  $\alpha = 0.25$ ,  $\beta = 0.5$ . All interfaces are prescribed as slip with interface-normal based artificial viscosity.

##### A. Kelvin-Helmholtz

Artificial surface tension inhibits instability growth and the Kelvin-Helmholtz test-case is often used as an example of this effect. Here we follow the test set up of Frontiere for the 2D Kelvin Helmholtz [16]. A high density band of gamma-law gas  $\rho = 2$ ,  $0.25 < y < 0.75$ ,  $\gamma = 5/3$  is initialized with an  $x$ -velocity of 0.5 and surrounded in either side by low density gas  $\rho = 1$ ,  $\gamma = 5/3$  in pressure equilibrium,  $P = 2.5$ , on a  $256 \times 256$  lattice. The  $y$ -velocity is initially perturbed sinusoidally  $v_y = 0.01 \sin(\pi x)$  to seed the instability.

Contour plots for the three different formulations at shown in Figs. 2 and 2 for times  $t = 4\tau_{KH}$  and  $t = 2\tau_{KH}$ . Traditional SPH (top) exhibits the characteristic surface tension effect suppressing rollup. At  $t = 2\tau_{KH}$  PSPH and FSISPH capture the role-up from the seeded initial instability as well as secondary structures. At  $t = 4\tau_{KH}$  PSPH and FSISPH show similar degrees of mixing. This particular PSPH run happened

to form with a modest asymmetry, but in general, FSISPH and PSPH do not differ qualitatively.

##### B. Rayleigh-Taylor

The Rayleigh-Taylor instability is encountered when a heavy fluid is supported by a light fluid within a gravitational field. Gamma-law gases  $\gamma = 5/3$  are again used for this test-case. The gravitational acceleration is set to 0.5. The density and pressure fields are initialized consistent with a state of hydrostatic equilibrium with a  $2 \times$  interface-density ratio and piecewise constant specific thermal energy. The densities at the interface are 1.0 and 0.5 for the heavy and light fluid respectively and the interface pressure is 2.5. The initial  $y$ -position is perturbed  $y = -0.01 \sin(2\pi x)$  to seed the instability.

Figure 4 shows density contours after 5-seconds. FSISPH (left) and PSPH (center) capture similar levels of detail with PSPH resolving slightly more fine structure. SPH only resolves the primary spike.

##### C. Blob Test

The Blob Test [1] tracks the instability-driven break-up of a high density blob when impacted by a low density supersonic flow. Traditional SPH formulations damp the instabilities and suppress the break-up. The problem is set with particles on a  $1024 \times 256$  lattice at low density  $\rho = 1$ . The high density,  $\rho = 10$ , blob is initially circular consisting of volume match particle organized in a circularly conformal distribution. The

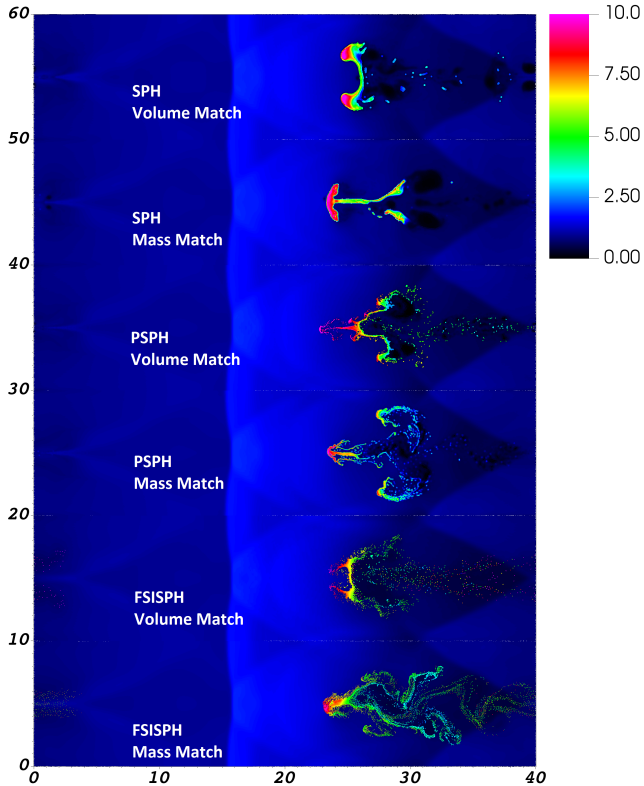


Fig. 5. Density contours for the Blob Test at  $t = 4\tau_{KH}$

blob is initially at rest and is subsequently accelerated by the low density medium traveling at Mach=1.6 in the positive  $x$  direction.

Figure 5

#### D. Shock-Water Column Interaction

The interaction of a shock wave with a water column, has been examined experimentally and numerically by a number of authors. Here we compare to the finite volume results of Xiang and Wang [17] who modeled the experiments of Sembian et. al. [18]. They created a 22-mm diameter by 5-mm tall water column and subjected it to a Mach 2.4 shock wave to examine the transient shock structure. Xiang and Wang validated their finite-volume code against these experiments but also ran simulations to later times at which the column begins to significantly deform under instability growth.

The initial conditions for the simulation are as follows: unshocked air ( $P = 1.01\text{-bar}$ ,  $\rho = 1.225\text{-kg/m}^3$ ,  $\gamma = 1.4$ ) is initialized in a lattice; the water column is in pressure equilibrium and discretized in a circularly conformal manner. Shocked air is initialized immediately upstream in a lattice that is mass-matched with the unshocked air. The state of the shocked air is derived from classic normal-shock relations  $M = 2.4$ ,  $P = 0.664\text{-MPa}$ ,  $\rho = 3.85\text{-kg/m}^3$   $v = 567\text{-m/s}$ . The volumes of the initially shocked air is set such that the sizes of the interacting water and air nodes are roughly equivalent

behind the column's bow-shock. air is modelled as a gamma-law gas and water is modelled using the stiffened-gas equation of state, Eqn. 28 with  $\gamma = 6.2$  and  $P_0 = 0.343\text{-GPa}$ . In the results presented here, resolution is set at 50 nodes per column radius.

$$P = (\gamma - 1)\rho u - \gamma P_0 \quad (28)$$

The sound speed of water is then given by Eqn. 29.

$$c^2 = \gamma(\gamma - 1)(u + P_0/\rho) \quad (29)$$

Xiang and Wang used a non dimensional time  $t^*$  defined in Eqn. 30, in which  $d_0$  is the initial column diameter and  $v$  is the speed of the shocked air.

$$t^* = \frac{t}{d_0}v \quad (30)$$

Results for our FSISPH implementation are shown in Fig. 6 for  $t = 13.60t^*$ . This corresponds to the last image in Fig. 4 on Xiang and Wang 2017 [17]. In the left-most image the phase is plotted illustrating the deformation of the water column. The phase boundary is compared to that of Ref. [17] in subfigure (c). Note, Xiang and Wang used a radius of 22-mm so our phase boundary is scaled 2× to get the overlay. Good agreement is seen with regards to overall shape, though the finite volume results appear to capture larger amplitude instabilities.

A contour of the pressure field is shown in the central subfigure. The pressure is smooth within each individual phase with a modest discontinuity at the interface. The air experiences an artificial pressure jump and the water a dip. A potential source of the oscillation is the assumed interface location between interacting pairs – i.e. the midpoint. In the case of an approaching water-air pair, the volumetric compression would be almost completely assigned to the air node. Upon the next iteration however, the new interface location has moved as if the compression was equally distributed. Over successive iteration this tends to cause the more pliable material to overcompress.

## V. DISCUSSION

A new fully conservative SPH formulation for multimaterial problems with large variation in material properties has been outlined. The new formulation was then applied to several classic SPH test problems, and compared to a result from literature for air-shock water column interactions. The new formulation does not exhibit the surface tension issue of classic SPH and performs similarly to PSPH on mixing tests. The general deformation of a water column subject to supersonic flow agrees relatively well with previous finite volume method results, though the FSISPH formulation still produces a pressure blip at the material interface.

## APPENDIX

An interface state, denoted by \* superscript, is constructed by applying the definition of the isentropic bulk modulus, Eqn.

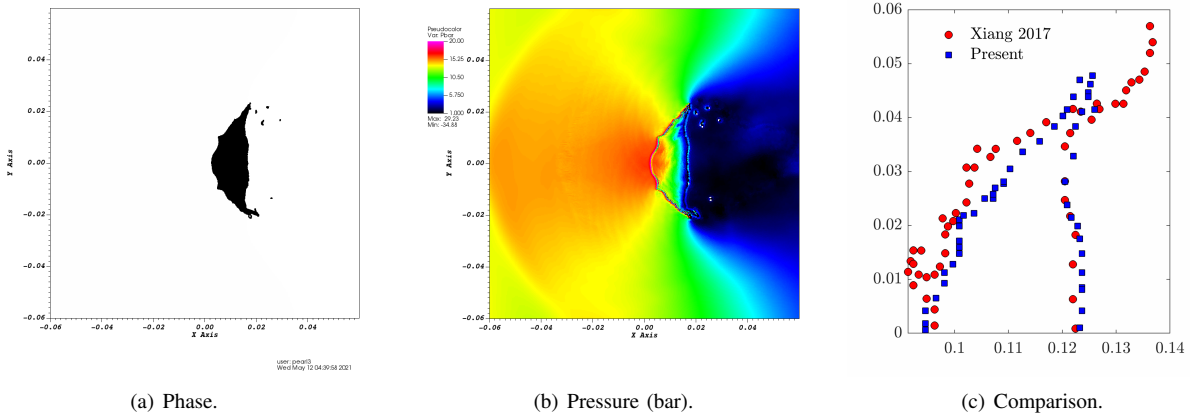


Fig. 6. Water column shock test  $t = 13.80t^*$  with phase boundary compared to results of Xiang and Wang 2017 [17].

31, to the node-pair interaction. The interface pressure is then required to be single valued, Eqn. 32.

$$K \equiv \rho \frac{\partial P}{\partial \rho} \Big|_S \quad (31)$$

$$\frac{K_i}{\rho_i} \frac{D\rho_i}{Dt} = \frac{DP^*}{Dt} = \frac{K_j}{\rho_j} \frac{D\rho_j}{Dt} \quad (32)$$

The contribution to the continuity equation from a pair interaction is written in Eqn. 33 in terms of the nodal velocity projected onto the line of action  $v_i^{\parallel}$  and the interface velocity along the line. Here the magnitude of the kernel gradient is used and as such the indicial subscript is dropped.

$$\frac{1}{\rho_i} \frac{D\rho_i}{Dt} = \frac{m_j}{\rho_j} (v_i^{\parallel} - v_*^{\parallel}) \nabla W_i \quad (33)$$

Substituting Eqn. 33 into Eqn. 32 and rearranging terms, the interface velocity along the line of action can be determined from the nodal velocities, bulk moduli, volumes, and kernel gradient magnitudes according to Eqn. 35. An intermediate result is present in Eqn. 34.

$$K_u V_j (v_i^{\parallel} - v_*^{\parallel}) \nabla W_i = -K_j V_i (v_j^{\parallel} - v_*^{\parallel}) \nabla W_j \quad (34)$$

$$v_*^\parallel = \frac{K_i V_j \nabla W_i v_i^\parallel + K_j V_i W_j v_j^\parallel}{K_i V_j \nabla W_i + K_j V_i \nabla W_j} \quad (35)$$

#### ACKNOWLEDGMENT

This work was performed under the auspices of the U.S. Department of Energy by Lawrence Livermore National Laboratory under Contract DE-AC52-07NA27344.

## REFERENCES

- 31, to the node-pair interaction. The interface pressure is then  
required to be single valued, Eqn. 32.

$$K \equiv \rho \left. \frac{\partial P}{\partial \rho} \right|_S \quad (31)$$

$$\frac{K_i}{\rho_i} \frac{D\rho_i}{Dt} = \frac{DP^*}{Dt} = \frac{K_j}{\rho_j} \frac{D\rho_j}{Dt} \quad (32)$$

The contribution to the continuity equation from a pair interaction is written in Eqn. 33 in terms of the nodal velocity projected onto the line of action  $v_i^\parallel$  and the interface velocity along the line. Here the magnitude of the kernel gradient is used and as such the indicial subscript is dropped.

$$\frac{1}{\rho_i} \frac{D\rho_i}{Dt} = \frac{m_j}{\rho_j} (v_i^\parallel - v_*^\parallel) \nabla W_i \quad (33)$$

Substituting Eqn. 33 into Eqn. 32 and rearranging terms, the interface velocity along the line of action can be determined from the nodal velocities, bulk moduli, volumes, and kernel gradient magnitudes according to Eqn. 35. An intermediate result is present in Eqn. 34.

$$K_u V_j (v_i^\parallel - v_*^\parallel) \nabla W_i = -K_j V_i (v_j^\parallel - v_*^\parallel) \nabla W_j \quad (34)$$

$$v_*^\parallel = \frac{K_i V_j \nabla W_i v_i^\parallel + K_j V_i \nabla W_j v_j^\parallel}{K_i V_j \nabla W_i + K_j V_i \nabla W_j} \quad (35)$$

### ACKNOWLEDGMENT

This work was performed under the auspices of the U.S. Department of Energy by Lawrence Livermore National Laboratory under Contract DE-AC52-07NA27344.

### REFERENCES

  - [1] O. Agertz, B. Moore, J. Stadel, D. Potter, F. Miniati, J. Read, L. Mayer, A. Gawryszczak, A. Kravtsov, . Nordlund, F. Pearce, V. Quilis, D. Rudd, V. Springel, J. Stone, E. Tasker, R. Teyssier, J. Wadsley, and R. Walder, “Fundamental differences between SPH and grid methods,” *Monthly Notices of the Royal Astronomical Society*, vol. 380, no. 3, pp. 963–978, 08 2007. [Online]. Available: <https://doi.org/10.1111/j.1365-2966.2007.12183.x>
  - [2] T. R. Saitoh and J. Makino, “A DENSITY-INDEPENDENT FORMULATION OF SMOOTHED PARTICLE HYDRODYNAMICS,” *The Astrophysical Journal*, vol. 768, no. 1, p. 44, apr 2013. [Online]. Available: <https://doi.org/10.1088/0004-637x/768/1/44>
  - [3] P. F. Hopkins, “A general class of Lagrangian smoothed particle hydrodynamics methods and implications for fluid mixing problems,” *Monthly Notices of the Royal Astronomical Society*, vol. 428, no. 4, pp. 2840–2856, 11 2012. [Online]. Available: <https://doi.org/10.1093/mnras/sts210>
  - [4] N. Hosono, T. R. Saitoh, and J. Makino, “Density-independent smoothed particle hydrodynamics for a non-ideal equation of state,” *Publications of the Astronomical Society of Japan*, vol. 65, no. 5, pp. 108–108, 2013.
  - [5] B. W. Ritchie and P. A. Thomas, “Multiphase smoothed-particle hydrodynamics,” *Monthly Notices of the Royal Astronomical Society*, vol. 323, no. 3, pp. 743–756, 05 2001.
  - [6] A. Colagrossi and M. Landrini, “Numerical simulation of interfacial flows by smooth particle hydrodynamics,” *Journal of Computational Physics*, vol. 191, no. 1, pp. 448–475, 2003.
  - [7] J. W. Wadsley, B. W. Keller, and T. R. Quinn, “Gasoline2: a modern smoothed particle hydrodynamics code,” *Monthly Notices of the Royal Astronomical Society*, vol. 471, no. 2, pp. 2357–2369, 06 2017. [Online]. Available: <https://doi.org/10.1093/mnras/stx1643>
  - [8] D. J. Price, “Modelling discontinuities and kelvinhelmholtz instabilities in sph,” *Journal of Computational Physics*, vol. 227, no. 24, pp. 10040–10057, 2008. [Online]. Available: <https://www.sciencedirect.com/science/article/pii/S0021999108004270>
  - [9] W. Benz and E. Asphaug, “Impact simulations with fracture. i. method and tests,” *Icarus*, vol. 107, no. 1, pp. 98 – 116, 1994.
  - [10] J. Owen, “A compatibly differenced total energy conserving form of sph,” *International Journal for Numerical Methods in Fluids*, vol. 75, no. 11, pp. 749–774, 2014. [Online]. Available: <https://onlinelibrary.wiley.com/doi/abs/10.1002/fld.3912>
  - [11] N. Grenier, M. Antuono, A. Colagrossi, D. Le Touzé, and B. Alessandrini, “An hamiltonian interface sph formulation for multi-fluid and free surface flows,” *Journal of Computational Physics*, vol. 228, no. 22, pp. 8380 – 8393, 2009.
  - [12] J. Monaghan and R. Gingold, “Shock simulation by the particle method sph,” *Journal of Computational Physics*, vol. 52, no. 2, pp. 374–389, 1983. [Online]. Available: <https://www.sciencedirect.com/science/article/pii/0021999183900360>
  - [13] “Asymmetries in extragalactic radio sources,” 1990.
  - [14] J. J. Monaghan, “Smoothed particle hydrodynamics,” *Annual Review of Astronomy and Astrophysics*, vol. 30, no. 1, pp. 543–574, 1992. [Online]. Available: <https://doi.org/10.1146/annurev.aa.30.090192.002551>
  - [15] W. Dehnen and H. Aly, “Improving convergence in smoothed particle hydrodynamics simulations without pairing instability,” *Monthly Notices of the Royal Astronomical Society*, vol. 425, no. 2, pp. 1068–1082, 09 2012. [Online]. Available: <https://doi.org/10.1111/j.1365-2966.2012.21439.x>
  - [16] N. Frontiere, C. Raskin, and J. Owen, “Crksph a conservative

- reproducing kernel smoothed particle hydrodynamics scheme,” *Journal of Computational Physics*, vol. 332, pp. 160–209, 2017. [Online]. Available: <https://www.sciencedirect.com/science/article/pii/S0021999116306453>
- [17] G. Xiang and B. Wang, “Numerical study of a planar shock interacting with a cylindrical water column embedded with an air cavity,” *Journal of Fluid Mechanics*, vol. 825, p. 825852, 2017.
- [18] S. Sembian, M. Liverts, N. Tillmark, and N. Apazidis, “Plane shock wave interaction with a cylindrical water column,” *Physics of Fluids*, vol. 28, no. 5, p. 056102, 2016.